p-Type PdO nanoparticles supported on *n*-type WO$_3$ nanoneedles for hydrogen sensing

F.E. Annanouch [a,b], S. Roso [a], Z. Haddi [a,c], S. Vallejos [d], P. Umek [e], C. Bittencourt [f], C. Blackman [g], T. Vilic [a], E. Llobet [a,*]

[a] Minos-EMaS, Universitat Rovira i Virgili, Avda. Països Catalans, 26, 43007 Tarragona, Spain
[b] Aix Marseille Université, CNRS, Université de Toulon, IM2NP UMR 7334, Marseille, France
[c] Laboratoire des Sciences de l'Information et des Systèmes (LSIS), Aix-Marseille University, France
[d] SIX Research Centre, Brno University of Technology, Technická 10, Brno, CZ-61600, Czech Republic
[e] Department of Solid-State Physics, Jožef Stefan Institute, Jamova cesta 39, 1000 Ljubljana, Slovenia
[f] Materia Nova, Univeristé de Mons, Parc Initialis - Av. N. Copernic, 1, B-7000 Mons, Belgium
[g] Department of Chemistry, University College London, 20 Gordon Street, London WC1H 0AJ, United Kingdom

ARTICLE INFO

ABSTRACT

We report the synthesis of palladium nanoparticle (NP) decorated WO$_3$ nanoneedles (NNs) employing a single-step, aerosol assisted chemical vapor deposition approach. Two different Pd precursors were investigated in view of optimizing the morphology and the gas sensing performance of the resulting nanostructured films. In particular, palladium acetylacetonate was found to be more suitable than ammonium hexachloropalladate for obtaining *n*-type WO$_3$ NNs uniformly decorated with well dispersed *p*-type PdO NPs. The active films could be directly deposited on the electrode area of microelectromechanical system-based resistive transducers. The morphology and chemical composition of the films was investigated by scanning electron microscopy, high-resolution transmission electron microscopy, Raman spectroscopy and X-ray photoelectron spectroscopy analysis. PdO-decorated WO$_3$ NNs show a response toward hydrogen that is about 680 times higher than that of bare WO$_3$ NNs. Finally, PdO-loaded sensors display extremely low-cross sensitivity to water vapor, which makes them remarkably immune to changes in the background humidity.

1. Introduction

Tungsten trioxide (WO$_3$), a transition metal oxide and *n*-type semiconductor has been employed in a wide spectrum of applications including electrochromic and photochromic devices [1,2], photocatalysis [3], and gas sensors [4]. With the development of nanotechnology, WO$_3$ has been synthesized in different forms such as nanoneedles [4], nanotubes [5], and nanorods [6]. In comparison to standard polycrystalline metal oxide films, nanostructured metal oxides provide higher surface-to-volume ratio, higher level of crystallinity or the presence of quantum confinement effects, which have improved gas sensitivity [7], and long term stability [4]. The development of synthesis techniques to achieve uniform size and shape, defect-free crystal structure and homogenous stoichiometry in nanostructures metal oxides is a technological challenge. The aerosol assisted chemical vapor deposition (AACVD) has been shown a suitable method for producing tungsten oxide nanoneedles (NNs) with remarkable gas sensing properties [7].

Additionally, AACVD has been employed for co-synthesizing, in a single step, tungsten oxide NNs homogeneously decorated with metal or metal oxide nanoparticles of Pt, Au or Cu$_2$O [4,8–10]. It is well known that the loading of the metal oxide matrix with catalyst nanoparticles (e.g., surface functionalization of the nanostructured metal oxide) may lead to significant improvements in response, selectivity, long-term stability and cross-sensitivity to ambient moisture. In particular Pd has been widely employed as sensitizer in metal oxide films for developing hydrogen sensors [11–13]. In this paper we explore the AACVD synthesis of Pd nanoparticle (NP)-decorated WO$_3$ NNs, using a single-step strategy, with two different palladium precursors (palladium(II) acetylacetonate and ammonium hexachloropalladate(IV)). Pd-decorated nanoneedles are directly grown onto microelectromechanical systems (MEMs) based micro-hotplate transducers in view of obtaining resistive hydrogen sensors.

Scanning electron microscopy (SEM), X-ray diffraction (XRD), high-resolution transmission electron microscopy (HRTEM), Raman spectroscopy and X-ray photoelectron spectroscopy (XPS) have been used to determine the morphology, phase composition, and microstructure of the layers grown. Once the best precursor is identified, the hydrogen

* Corresponding author.
  E-mail address: eduard.llobet@urv.cat (E. Llobet).

sensing properties of both bare and Pd decorated WO_3 NNs are discussed in detail. Special attention is paid to the effect of background humidity in sensor response.

2. Experimental

2.1. Transducer platforms

MEMS-based microsensor platforms employed a double side polished *p*-type (100) Si substrate with 300 μm thickness. The microfabrication steps comprised implantation, photolithography, metallization, lift-off and back side etching of the substrate to define the membranes. In one chip, four membranes with dimension of 1 mm × 1 mm, were grown. Each membrane (see Fig. 1) comprised of a $POCl_3$-doped polysilicon resistive heater (16 Ω/sq., 0.47 μm thickness, and TCR = 6.79×10^{-4}/°C), silicon oxide insulator layer (800 nm thick), and platinum electrodes (0.2 μm thickness, 50 μm electrode gap). Each chip was mounted on a standard TO-8 package [7]. During AACVD, a shadow mask was used to confine the film deposition to the electrode area.

2.2. Reactants

Palladium(II) acetylacetonate (99%), Ammonium hexachloropalladate(IV) (99,99%), Tungsten hexacarbonyl (97%), Methanol (≥99.9%), Ethanol (≥99.8%) and Acetone (≥99.9%) were obtained from Sigma-Aldrich and were used as received without further purification.

### 2.3. Synthesis procedure

The synthesis was carried out in a horizontal AACVD reactor using N_2 (g) (99.96%, BOC) as a carrier gas (300 sccm). A Johnson Matthey Liquifog 2 operating at 2 MHz was used to generate the aerosol from the precursor solutions. In a previous step, MEMS microsensors substrates were cleaned with acetone, then with ethanol, dried with air and then placed inside the reactor. Pure WO_3 NNs were obtained at 500 °C, from AACVD of $W(CO)_6$ (50 mg) dissolved in a mixture of acetone (15 cm^3) and methanol (5 cm^3). One set of Pd nanoparticle decorated WO_3 NNs were synthesized at 400 °C via a single-step AACVD co-deposition route with $W(CO)_6$ (50 mg) dissolved in acetone (15 cm^3) and [Pd(acac)$_2$] (5 mg) dissolved in methanol (5 cm^3). This sample is denoted **ac-1SD**. A second set of Pd nanoparticle decorated WO_3 NNs were synthesized at 400 °C via a single-step AACVD co-deposition route with $W(CO)_6$ (50 mg) dissolved in acetone (15 cm^3) and $(NH_4)_2PdCl_6$ (5.8 mg) dissolved in methanol (5 cm^3). This sample is denoted **am-1SD**. It is worth noting that the co-deposition with $(NH_4)_2PdCl_6$ was difficult due to the low solubility of this precursor in acetone. After deposition all samples were subjected to annealing at 500 °C for 3 h in air. Table 1 summarizes the growth conditions.

2.4. Material analysis tools

Scanning electron microscopy (SEM) images were taken using the FEI Quanta 600. XRD patterns were collected by Bruker, AXD D8-Discover, using Cu K-α radiation operated at 40 kV and 40 mA. Raman spectra were obtained employing a Renishaw Raman Fourier transform infrared spectrometer. High resolution transmission electron microscopy images were obtained from a JEOL JEM-2100 with a LaB_6 filament at an acceleration voltage of 200 keV. Film samples were prepared by removing the film from the glass substrate via sonication in methanol for 15 min, and then drop-casting onto an Agar Scientific 400 Cu mesh holey carbon grid. Excess solutions were removed with filter paper. Images were recorded on a Gatan Orius charge-coupled device. XPS analysis of the films was carried out using a Thermo Scientific Kα spectrometer with Al K-α radiation, a dual beam charge-compensation system, and constant pass energy of 50 eV. All the XPS data were elaborated using Casa XPS *v*.2.3 software and binding energies were referenced with respects to C1s peak at 284.5 eV.
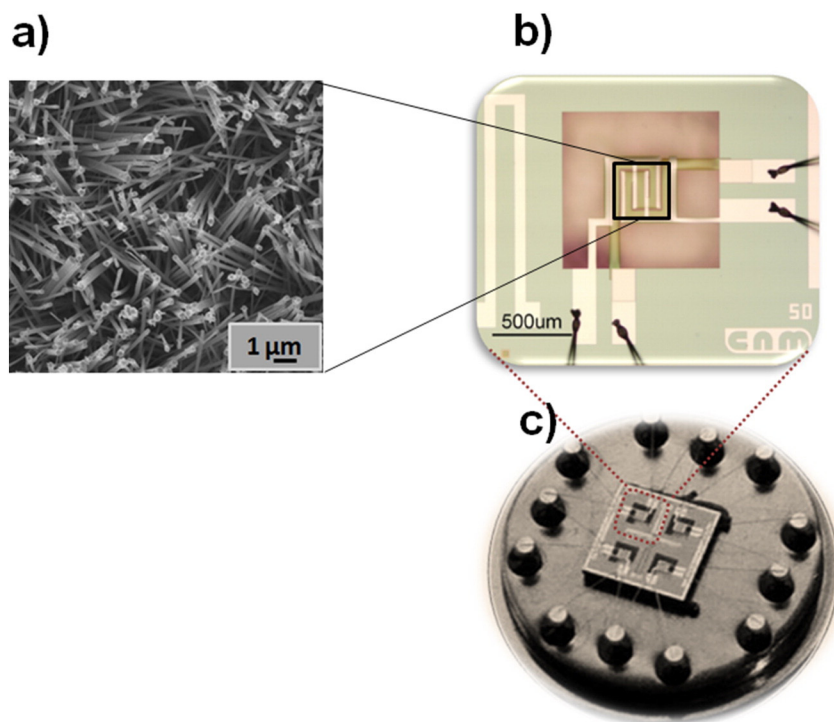
Fig. 1. SEM image of the sensing film (a); photograph of an individual microsensor platform showing the sensing-active area (b) and array of microsensors mounted on a standard TO-8 package (c).